ACS Photonics

Article

pubs.acs.org/journal/apchd5

Plasmonic Scattering Back Reflector for Light Trapping in Flat Nano-Crystalline Silicon Solar Cells

Lourens van Dijk,*[,†] Jorik van de Groep,[‡] Leon W. Veldhuizen,[§] Marcel Di Vece,[†] Albert Polman,[‡] and Ruud E. I. Schropp[§]

[†]Utrecht University, Nanophotonics - Physics of Devices, Debye Institute for Nanomaterials Science, High Tech Campus, Building 21, 5656 AE Eindhoven, The Netherlands

[‡]FOM Institute AMOLF, Center for Nanophotonics, Science Park Amsterdam 104, 1098 XG Amsterdam, The Netherlands

[§]Eindhoven University of Technology (TU/e), Department of Applied Physics, Plasma and Materials Processing, 5600 MB Eindhoven, The Netherlands

Supporting Information

ABSTRACT: Most types of thin film solar cells require light management to achieve sufficient light absorptance. We demonstrate a novel process for fabricating a scattering back reflector for flat, thin film hydrogenated nanocrystalline silicon (nc-Si:H) solar cells. This scattering back reflector consists of an array of silica nanocylinders in a metal sheet. Typically, nc-Si:H solar cells are grown on textured substrates that scatter the incoming light. However, one needs to make compromises to the size and aspect ratio of the scattering features and the material growth process to prevent growth defects in the nc-Si:H layers on top of such (nano)-structured substrates. Here, we grow a high-quality nc-Si:H layer on a flat superstrate. On top of this, we apply a plasmonic scattering structure composed of a periodic array of dielectric nanocylinders, which is overcoated by silver. The use of a flat plasmonic scattering back reflector (PSBR) circumvents silicon growth defects and prevents the associated reduction of the open circuit voltage, while on the other hand, the scattering improves the short circuit current. The PSBR is fabricated over a large area using substrate conformal imprint lithography (SCIL). Optical modeling was performed using finite-difference time-domain (FDTD) simulations to determine the absorptance in the active layer of the cell. A particle swarm optimization algorithm is used to optimize the PSBR geometry, such that the photocurrent is maximized. We fabricated a 1 μm thick nc-Si:H cell and experimentally demonstrate a current improvement of 32% compared to a flat reference cell, without affecting the open circuit voltage. The PSBR structure is shown to be effective for nc-Si:H solar cells, and the concept of flat scattering back reflectors is compatible with a wide range of other thin film superstrate solar cells.

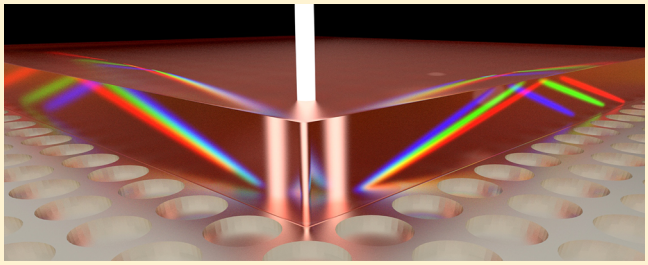

KEYWORDS: *photovoltaics, light management, solar energy, plasmonic scattering, nanocrystalline silicon, FDTD, imprint lithography*

The flexibility and low cost of thin film solar cells makes them attractive for a wide range of applications, such as building integrated photovoltaics[1] and power generation mobile devices. However, the design of these cells is challenging, as there is a conflicting interplay between their electrical and optical properties. From the optical perspective, a thick solar cell is ideal, while from the electrical and cost perspective a thin cell is beneficial. This dilemma can be solved by improving the diffusion length of the charge carriers, or by improving the absorptance.

Like many thin film solar cells, hydrogenated nanocrystalline silicon (nc-Si:H) suffers from this opto-electrical dilemma.[2,3] Thick (>2 μm) nc-Si:H solar cells have a lower open circuit voltage (V_{oc}) and fill factor (*FF*) and require a relatively long fabrication time.[4] Thin cells (~1 μm) have been shown to have ~4% higher V_{oc} and ~7% higher *FF*, but they only absorb a small fraction of the solar spectrum.[4,5] The J_{sc} of the record-efficiency nc-Si:H cell is only 67% of the limiting value given by the Shockley-Queisser model,[6,7] one of lowest fractions of all major solar cell materials. Therefore, light trapping is required to enhance the optical absorption in thin nc-Si:H solar cells, especially for long wavelengths (λ > 600 nm).

Efficient light trapping inside the cell has been demonstrated by depositing the solar cell on textured substrates, like textured aluminum-doped zinc oxide[8−10] ZnO nanorods on flat silver,[11] textured Ag films[12] and honeycomb patterns.[10,13] However, growing nc-Si:H on nanotextured substrates commonly results in growth defects, apparent as voids, short-circuiting pinholes and cracks in the nc-Si:H layer, which increase the charge carrier recombination rate and can even lead to excessive shunting.[10,14−18] On the contrary, layers grown on flat substrates do not show such defects, but they are hindered by a lack of light trapping. The best of both worlds can be achieved by applying a light scattering layer onto a flat high-quality nc-Si:H layer. This

Received: January 29, 2016
Published: March 25, 2016

DOI: 10.1021/acsphotonics.6b00070
ACS Photonics 2016, 3, 685−691

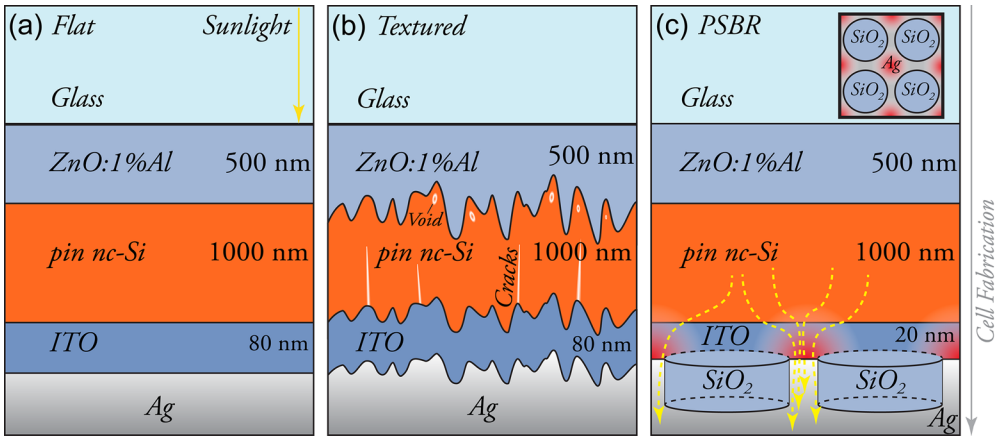

Figure 1. Illustration of the fabricated solar cells. (a) Flat nc-Si:H solar cell. (b) nc-Si:H cell grown on top of textured aluminum-doped ZnO. Voids can occur due to the texture. (c) Flat cell with a plasmonic scattering back reflector (PSBR) consisting of a square array of SiO_2 nanocylinders in a matrix of Ag. The dashed yellow lines sketch the electrical path of the electrons via the conductive Ag. The red circles illustrate the plasmonic scattering by the PSBR. The inset shows a top view of the flat PSBR.

combination facilitates both the electrical and optical requirements and can therefore result in high cell performance. Another advantage of the flat architecture is that nc-Si:H can be grown at higher deposition speeds on flat substrates than on textured substrates, without inducing excessive material defects.[19,20] The flat interfaces in the PSBR cell reduce the surface area and associated surface recombination.[21] To prevent cracks from occurring, one can use large-scale (~micrometer-sized) features, which is, however, a compromise between light scattering and material quality.[10]

Recently, light trapping in flat substrate solar cells has been demonstrated using the flattened light-scattering substrate (FLiSS) concept.[5,21] For the FLiSS cell, a composite of two dielectric materials (such as ZnO and amorphous Si) is flattened by chemical mechanical polishing, after which a flat nc-Si:H layer is grown on top. However, the FLiSS concept is not suitable for superstrate cells, which are industrially more interesting as the front glass offers high transparency, UV stability, and moisture protection.[22]

Here, we present a plasmonic scattering back reflector (PSBR) that provides efficient light trapping in flat absorber layers, in the superstrate cell configuration. The PSBR is similar to a plasmonic hole array, which is known to support surface plasmon resonances,[23] which can result in strong local electric fields inside the voids,[24] and have a large scattering cross section with a tunable resonance wavelength.[25−27] The benefits of such hole arrays have been successfully demonstrated in substrate solar cells of which the deposition is not significantly hindered by surface textures, for example, organic[28] and a-Si solar cells.[29,30]

First, a crack-free nc-Si:H p-i-n solar cell is grown on flat, ZnO-coated glass. Next, a square array of dielectric nanocylinders is printed on the backside of the flat silicon layer by substrate conformal imprint lithography (SCIL),[29,31] which is subsequently overcoated by silver to form the PSBR. Plasmonic scattering by imprinted metal nanoparticles embedded in a dielectric has been demonstrated before on substrate cells;[29,32,33] here, we demonstrate plasmonic scattering by a metal film with cylindrical silica "nanoparticles" in a superstrate solar cell. The geometric structure and the refractive index contrast between the metal and the silica give rise to efficient plasmonic scattering and reduces optical losses. Replacing the SiO_2 nanocylinders by a dielectric with higher refractive index could result in stronger scattering. However, higher index materials also tend to have more parasitic absorptance, and it is more difficult to integrate such material in our imprint procedure.

The generated photocurrent of a thin nc-Si:H PSBR cell is compared to that of two reference cells: a flat reference cell and a reference cell deposited on a textured superstrate. Due to scattering by the PSBR, the J_{sc} improves by 3.7 mA/cm^2 with respect to the flat reference cell. The V_{oc} of the PSBR cell is comparable to that of the flat reference cell, while the textured reference cell showed, as expected, a reduced V_{oc} due to cracks. The results demonstrated here are generic and can be applied to a wide variety of thin film, superstrate solar cells.

DESIGN AND FABRICATION OF THE SOLAR CELLS

We compare three different cell designs as shown in Figure 1. The three designs incorporate nc-Si:H p-i-n layers grown on a glass superstrate. The thickness of the intrinsic nc-Si:H layer is ~1 μm. The cells have an optically thick Ag layer at the backside, which functions both as a back reflector and contact. The fabrication details are provided in the Supporting Information. Figure 1a shows the flat reference cell in which light travels through the cell without being scattered (except some scattering on the grain boundaries). The flat design allows for high material quality. The textured reference cell (Figure 1b) is grown on textured aluminum-doped zinc oxide (ZnO:Al). The different growing crystal facets approach one another without forming a good physical interconnection, as indicated by the short-circuiting pinholes. Due to the (partially) conformal growth on top of the random front texture, the interfaces between subsequently deposited layers are also textured and, thereby, scatter the incident light. An 80 nm thick ITO layer ($n \sim 2.1$) is used as a back dielectric spacer to achieve a high E-field in the Si layer.[34] Figure 1c shows the cell with the PSBR at the backside. The PSBR is applied on a flat nc-Si:H layer. The PSBR is an array of silica (SiO_2, $n \sim 1.46$) nanocylinders overcoated with silver. A 20 nm thick continuous layer of indium tin oxide (ITO) forms an etch barrier between the nc-Si:H layer and the PSBR. This thickness can be further reduced for improved device performance. The conductive silver in between the silica nanocylinders is used to contact the cell, similar to the contacting scheme of the passivated emitter with rear locally diffused (PERL) cell.[35] The size and geometry of the nanocylinders array were optimized for

DOI: 10.1021/acsphotonics.6b00070
ACS Photonics 2016, 3, 685−691

maximized scattering into the nc-Si:H layer using numerical simulations.

Figure 2a illustrates the SCIL procedure to fabricate the PSBR. First, a master pattern is fabricated on a c-Si wafer using laser interference lithography. This patterned wafer can be used to produce a multitude of stamps and imprints. Next, a stamp is fabricated from this master which consists of a bilayer of two different types of soft polydimethylsiloxane (PDMS) and allows large-area replicability.[36,37] A layer of liquid silica (sol−gel) is subsequently spin-coated on top of the ITO backside of the solar cell and the SCIL stamp is applied. After 30 min of curing at ambient conditions, the sol−gel has solidified and the stamp is removed resulting in a silica nanopattern on the substrate.

A thin residual layer of silica remains in between the silica nanocylinders, which is removed using a CHF_3 based reactive ion etch (RIE). Figure 2b shows a scanning electron microscopy (SEM) top view image of the imprinted silica nanocylinder array. The imprint shows only a few defects.

Figure 2c shows a SEM image of a focused-ion beam (FIB) cross section of the PSBR. The nanocylinders have a diameter of ∼240 nm, a pitch of ∼325 nm, and a height of ∼70−90 nm. The metal covers ∼57% of the total area. The imprinted nanocylinders are slightly tapered as a result of the nonperfect anisotropy of the RIE. Due to semiconformal growth,[18] the shape of the nanoimprinted cylinders propagates through the evaporated Ag layer resulting in half dome like shapes at the surface of the Ag. Finally, a thin layer of aluminum is applied by thermal evaporation to prevent oxidation of the Ag layer.

RESULTS AND DISCUSSION

We determined the performance of the fabricated solar cells by measuring the current density versus voltage ($J-V$) characteristic, *EQE*, and optical absorptance. Figure 3 shows the measured $J-V$ characteristics of the flat, textured, and PSBR solar cell under AM1.5G illumination.

The flat nc-Si:H cell shows the highest *FF* of the three cells. However, the current is relatively low as light escapes from the cell due to poor light trapping. The textured cell shows a slightly higher short circuit current (J_{sc}) than the flat cell due to the light scattering at the textured interfaces. The V_{oc} is significantly lower compared to the flat reference cell as a result of the poor material quality due to growth defects induced by the texture. The strongly increased charge carrier recombination can also reduce the *FF* and J_{sc}. This demonstrates that wet chemically etched textures can have drawbacks on the growth and material quality of nc-Si:H cells, although we acknowledge that others developed sophisticated textures to remedy this problem.[6,10]

The PSBR solar cell shows the best performance. The J_{sc} improved by 3.7 mA/cm^2 with respect to the flat reference cell, which indicates efficient scattering into the active layer. The efficiency of the PSBR cell is 4.1%, which is significantly higher than the 3.5% of the flat reference cell. Moreover, these results demonstrate that the current is effectively transported through the narrow conductive silver paths in between the silica nanocylinders. Although the cell performance is slightly hindered by shunt resistance, it is important to highlight that the shunt resistance of the PSBR cell is similar to that of the flat reference cell, while the shunt resistance of the textured reference cell dropped significantly due to the poor material quality. The *FF* of the PSBR cell is lower than that of the flat cell. We indicate two potential issues: (1) damage to the ITO layer during the PSBR fabrication and (2) nonoptimal (partly lateral) conductivity from the nc-Si:H, via the ITO, toward the Ag terminals. Finally, the V_{oc} of the PSBR cell equals that of the flat cell, which demonstrates the benefit of flat, high quality nc-Si:H layers. We note that the overall efficiency of the cells used in this study is relatively low due to the relatively low nc-Si:H quality. Others reported a current of 17.5 mA/cm^2 for flat substrate based cells[4] and 23 mA/cm^2 for textured superstrate cells.[10] However, they serve as a good model system as all cell geometries were made using highly reproducible deposition conditions.

Spectral Performance: *EQE* and Absorptance. To investigate the current enhancement of the PSBR cell in more detail we measured the spectral performance of the completed cells. Figure 4 shows the absorptance and the external quantum efficiency (*EQE*) of the flat, textured, and PSBR solar cell.

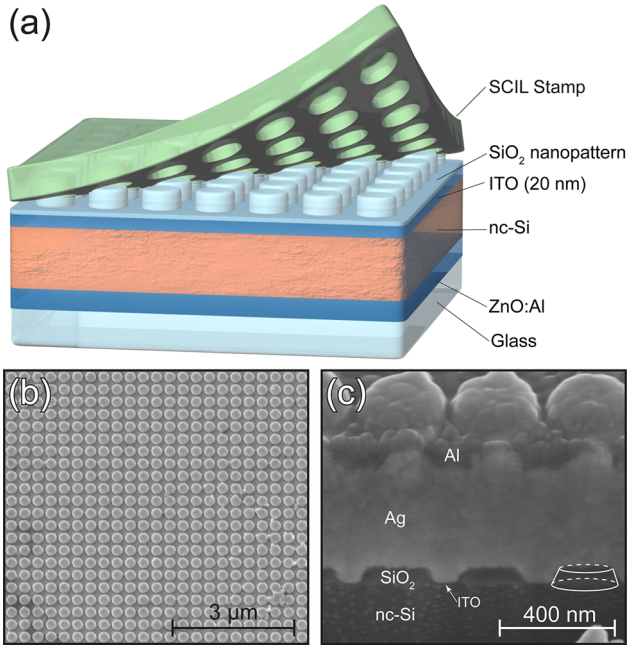

Figure 2. (a) Illustration of the soft conformal imprint lithography used to fabricate a square array of nanocylinders. (b) Top view SEM image of the imprinted silica nanocylinders. (c) SEM image of a FIB cross section of the PSBR solar cell.

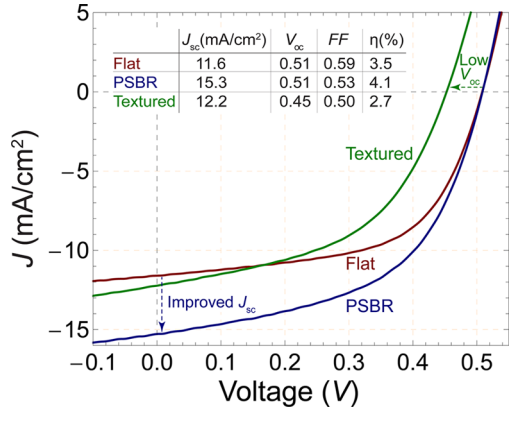

Figure 3. Measured current density vs voltage of the flat (red), textured (green), and PSBR (blue) solar cell under AM1.5G illumination. An improvement of 3.7 mA/cm^2 of the short circuit current density of the PSBR cell is observed compared to the flat cell, while the V_{oc} is identical.

DOI: 10.1021/acsphotonics.6b00070
ACS Photonics 2016, 3, 685−691

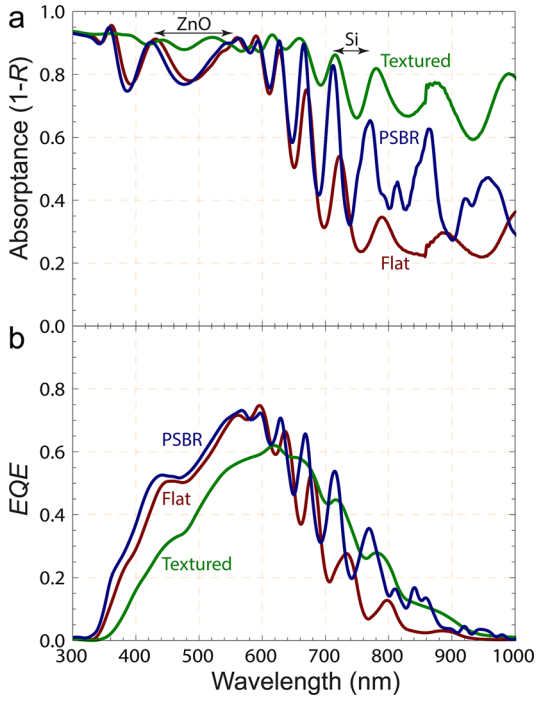

Figure 4. (a) Absorptance $(1 - R)$ and (b) the *EQE* of the flat cell (red), the PSBR cell (blue), and the textured solar cell (green). The *EQE* is measured at 0 V, without bias light. There is a small artifact in the absorption $(1 - R)$ data at ~860 nm due to a change of grating in the setup.

The flat cell shows 80–90% absorptance at short wavelengths (<600 nm). Due to parasitic absorptance in the *p*-type doped nc-Si:H layer, the *EQE* is significantly lower than the absorptance in this spectral range. For longer wavelengths, the absorptance drops to around 30%. Fringes appear due to Fabry-Pérot interference in the front ZnO:Al layer (for wavelengths < ~550 nm) and in the optically thick Si layer (at longer wavelengths).

The textured cell shows a high absorptance of 60–90%, even at the long wavelengths where the nc-Si:H is only weakly absorbing. However, the *EQE* is relatively low compared to the absorptance, especially at short wavelengths. We attribute this to poor internal collection efficiency (*ICE*) of the charge carriers generated at the top of the solar cell. This low *ICE* reflects the difficulty of growing high quality nc-Si:H layers on the texture, leading to material defects such as cracks.[10,14–18] See Supporting Information for a figure of the *IQE*. Moreover, sharp features in the surface of the metal contact layer lead to strong parasitic plasmonic absorption.[38] Another loss mechanism that is enhanced by the texture originates from the prolonged optical path through the parasitically absorbing *p*-layer as a result of the scattering by the front texture. The amplitude of the fringes in the *EQE* is significantly reduced compared to that of the flat cell. This is due to the randomization of the wave vectors inside the cell caused by random scattering at the textured interfaces. Texturing the front ZnO:Al layer induces scattering not only at the front interface, but also at the consecutive nc-Si:H/ITO/Ag interfaces due to the semiconformal growth of the subsequent layers. The absorptance of the PSBR cell at long wavelengths is lower than that of the textured cell. This is partly due to improved light incoupling at the ZnO/Si interface and the better light scattering at the three material interfaces of the textured cell. The random interface facilitates scattering over a broad spectral range. However, even though the absorptance is better, the device performance of the textured cell is worse.

The PSBR cell exhibits the highest overall *EQE*. Due to the light trapping, both the absorptance and the *EQE* are significantly higher than those of the flat cell for wavelengths longer than 700 nm. Above 750 nm the wavelength difference between a minimum and maximum of an (thickness related) interference fringe of the flat cell is at least 30 nm. It is observed that the PSBR cell has additional peaks on top of these fringes; the peak width is in the order of 10 nm. These peaks are attributed to additional resonances caused by the PSBR and are discussed in the next section.

Optical Modeling and Simulated Absorptance in Silicon Absorber. We used finite-difference time-domain (FDTD) simulations to obtain a detailed understanding of the optical mechanisms involved in the scattering and the wave-guiding in the PSBR cell. The geometry of the PSBR solar cell was optimized using the particle swarm optimization algorithm (PSO), see Supporting Information. We found the following optimal parameters of the square array of silica nanocylinders for the PSBR cell: a diameter of 248 nm, a pitch of 339 nm, and a height of 139 nm. Due to experimental constraints, the realized PSBR geometry differed from the calculated optimum; the realized height is around 70–90 nm. The short circuit current of the experimentally realized PSBR with suboptimal dimensions is only ~0.4 mA/cm^2 lower than that of the simulated optimum. The PSO algorithm also showed that for optimal absorptance in the intrinsic Si layer, the ITO should be as thin as possible. The light trapping due to scattering by the PSBR is better when the light is scattered in, or close to, a material with a high refractive index such as Si, as this gives rise to larger scattering angles. Also, the PSBR gives rise to strong field intensity in the near-field of the PBSR, and therefore, it is beneficial to have the Si layer very close to the PSBR.

We also simulated the absorptance of the PSBR cell with the experimentally realized geometry. Figure 5 shows the absorptance in the intrinsic nc-Si:H layer of the flat and the PSBR solar cell. As the ITO of the PSBR cell is 60 nm thinner than that of the flat cell, the thickness related interference fringes of the PSBR cell between 500 and 600 nm are slightly shifted to shorter wavelengths.

For long wavelengths, the PSBR cell shows a significant increase in absorptance. Generally, when a rough scattering layer

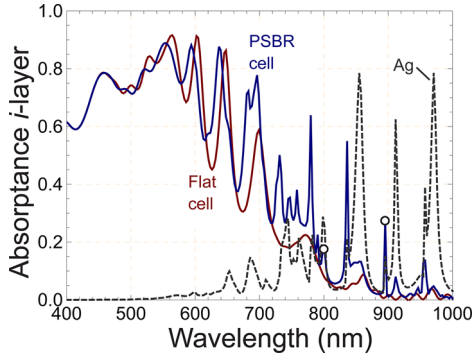

Figure 5. Simulated absorptance within the intrinsic layer of both the flat cell (red) and PSBR solar cell (blue). Sharp absorptance peaks are observed in the PSBR cell. The dashed line shows the total absorptance in the structured Ag of the PSBR cell. The circles mark some absorptance peaks for which both the *i*-layer and the PSBR structure have a corresponding wavelength.

DOI: 10.1021/acsphotonics.6b00070
ACS Photonics 2016, 3, 685–691

is applied, the light is randomized and thereby these fringes are smoothened. Here, distinct absorptance peaks appear on top of the Fabry-Pérot interference fringes which are strongly correlated to increased absorptance in the Ag nanostructure of the PSBR. These additional sharp peaks are due to a complex interplay between the PSBR and the cell caused by a combination of wave-guiding, interference, and scattering, as we discuss in the next section.

Resonances in the PSBR Solar Cell. To obtain a detailed understanding of the absorption in the cell, cross sections of the electric field intensity ($|E^2|$), and separate field components are shown at two distinct absorptance peaks in Figure 6a,d. The intensity profiles indicate a complex interplay of different resonance mechanisms. Therefore, we also plotted the E_x and E_z component ($E_y = 0$), see Figure 6b,c, and e,f, respectively. The E_x component at 801 nm reveals a strong E-field within the nanocylinder, while this is not the case at 895 nm. This has a strong effect on the profile of the E-field within the Si. Interestingly, a "checkerboard" pattern arises in the E_z field plot. The E-field of the incident light is directed along the x-axis, so E_z is zero. Therefore, a strong E_z component indicates lateral propagation through the solar cell, which indicates coupling to waveguide modes.

Above each silica nanocylinder there are two rows of extremes of the electric field. Due to the periodic grating of the PSBR the scattering pattern has a well-defined set of spatial frequencies. As a result, only a subset of the eigenmodes in the cell structure can be occupied, namely those which have an in-plane wave vector (k_x) that matches the periodic pattern of the PSBR. The conservation of the in-plane momentum dictates that these eigenmodes have an integer number of wavelengths in each unit cell of the grating.

Optical Scattering Processes and Interference Phenomena in the PSBR Solar Cell. The interaction of an electromagnetic wave with the PSBR in a nc-Si:H solar cell involves several (wavelength-dependent) interference and scattering phenomena, which form the origin for light trapping. Figure 7a shows scattering of light by a single particle. For a periodic array of scatterers, the interference of the scattered light results in a diffraction pattern, see Figure 7b. In the far field, light is diffracted according to the grating equation with several grating constants, including the pitch (p) and the diagonal pitch ($\sqrt{2}p$). For periodic arrays, the scattering is a superposition of the scattering by both the Ag pattern and the silica nanocylinders. Figure 7c illustrates three phenomena. First, light is attenuated as it propagates through the Si layer, and so the interaction with the PSRB is determined by the fraction of the light that is not absorbed in a single cell pass. Second, the cell is an optical resonator and supports Fabry-Pérot interference modes. Third, the electromagnetic field distribution inside the cylinders depends on the wavelength.

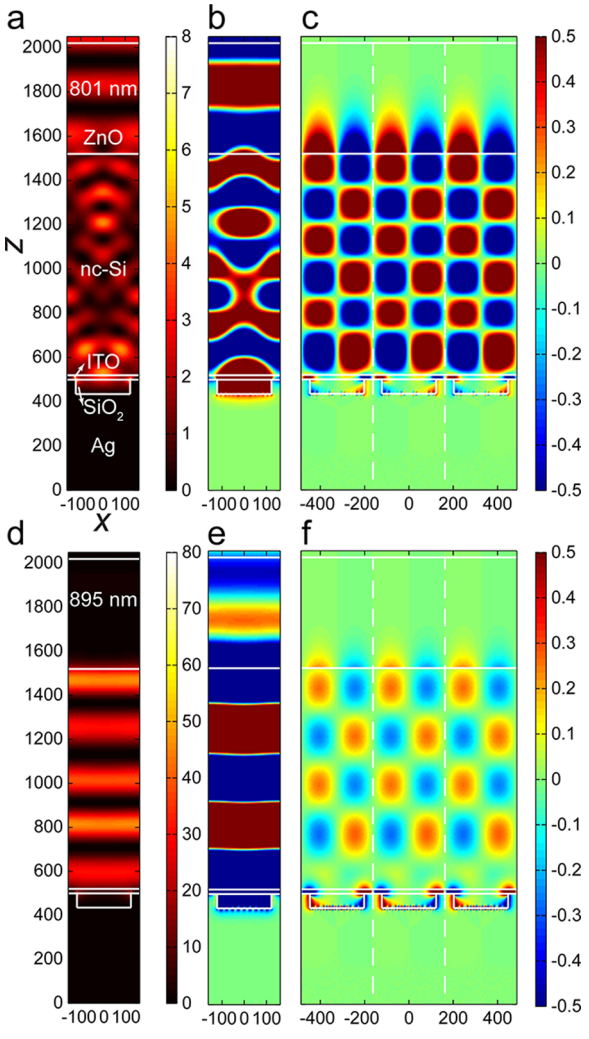

Figure 6. Plots of (a, d) $|E|^2$ in units of $(V/m)^2$, (b, e) real part of E_x, and (c, f) real part of E_z in (V/m) at two strong absorbing wavelengths: (a–c) $\lambda_0 = 801$ nm and (d–f) at $\lambda_0 = 895$ nm. The interfaces of the different materials in the cell are indicated by white lines. E_z is plotted for three unit cells, a characteristic checkerboard pattern arises due to scattering and wave guiding.

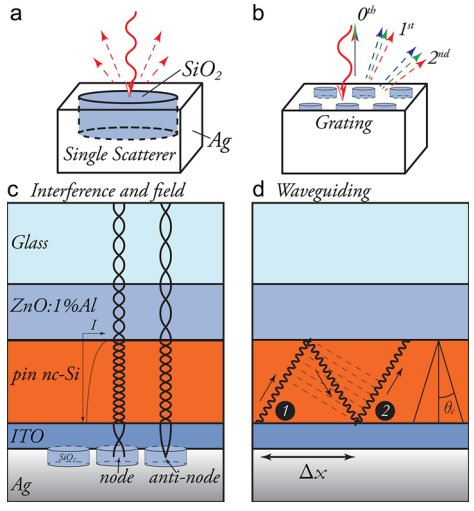

Figure 7. Simplified overview of the different scattering and interference mechanisms involved in the solar cell with a PSBR. (a) Single particle spatially scatters light to the active layer. (b) Array of these scattering particles gives rise to diffraction of light into the active layer. (c) Layer structure of the cell supports Fabry-Pérot resonances, leading to fringes in the absorptance spectrum. (d) Ray optics representation of waveguiding in the nc-Si:H solar cell. Light is totally internally reflected when the angle of incidence exceeds the critical angle θ_c. Waveguiding occurs if the indicated rays (**1**) and (**2**) interfere constructively. Each waveguide mode propagates at a specific mode angle within the thin Si slab, although only a subset of the available guided modes is populated in the PSBR cell.

DOI: 10.1021/acsphotonics.6b00070
ACS Photonics 2016, 3, 685–691

Figure 7d illustrates waveguiding in the silicon layer. The supported optical modes are determined by the thickness of the Si layer and the cladding layers.[39] When the planar component of the wave vector of light scattered into a specific mode matches to a grating constant of the PSBR array, light is efficiently coupled into such a mode and strong absorptance occurs in the active layer.

Small deviations in cell thickness and refractive index will drastically change the resonance conditions in the cell, thereby the absorptance peaks will shift significantly. This explains the observed difference between the peak width and wavelength between the simulated and experimental data. However, the simulations help to comprehend the complex interplay between the indicated optical phenomena, which results in the sharp absorptance peaks which we observed both in the experimental data and in the simulated absorptance (Figure 5). The resonances of an individual particle are spectrally broad.[31] The amplitude and width of the Fabry-Pérot resonances are determined by the interface reflectivity and cell thickness, respectively. In contrast, the width of the modal coupling resonances is determined by constructive interference along the waveguide over the modal absorption length. At long wavelengths, this leads to sharp coupling peaks due to the low absorption in the *i*-layer. In the experiment, local variation in cell parameters (mainly cell thickness) and the use of a light source with a certain spectral bandwidth (~10−15 nm) result in smoothening of the absorptance peaks, leading to broader observed absorptance maxima as experimentally observed.

Interestingly, it appears that enhanced absorptance in the *i*-layer of the PSBR solar cell coincides with enhanced absorptance in the Ag of the PSBR (e.g., see matching at wavelengths of 800, 838, 895, and 958 nm in Figure 5). This indicates resonant coupling between the PSBR and guided modes, leading to enhanced absorptance in the *i*-layer. This observation of scattering by nanocylinders in a metal film complements earlier observations of plasmonic resonances induced by metal nanoparticles.[29,32,40] Due to the strong resonant interaction with the PSBR, the absorptance in the PSBR also increases (up to 80%). Detailed analysis of the field profiles at the absorptance peaks showed that over 85% of the absorptance by the PSBR is absorbed in the Ag due to plasmonic resonances; the ITO and SiO_2 show only weak absorption.

Outlook. In this first exploration, we used a periodic pattern of nanocylinders. Semirandom patterns exhibit a broader range of spatial frequencies, which can broaden the absorptance peaks, resulting in a higher average absorptance[27,41−43] and reduced angular sensitivity.[44] Additional methods, such as external light trapping,[45] can improve the incoupling at the front side of the solar cell. The PSBR concept can also be interesting for other thin film superstrate solar cells.

CONCLUSIONS

We demonstrate a novel design and fabrication process for light trapping in thin film superstrate solar cells. This method is particularly suited to grow nc-Si:H of high material quality. In contrast to conventional structures for light scattering in solar cells, our plasmonic scattering back reflector (PSBR) does not involve texturization and, thereby, prevents growth-induced material defects. The PSBR is fabricated by soft-imprint lithography, which enables large-scale fabrication at low costs. The fabrication process does not involve any mechanical polishing step and can be applied at the backside of any superstrate cell. The particle swarm optimization algorithm is used to determine the optimal size of the silica nanocylinder array embedded in Ag. Using simulations, we identified the optical scattering mechanisms that give rise to the experimentally observed sharp absorptance peaks and the enhanced *EQE*. The PSBR shows an improved absorptance compared to the flat reference cell, without impacting the V_{oc}. The demonstrated scattering by cylindrical openings in a metal film complements previous reports on plasmonic scattering by metal nanoparticles. The demonstrated processing method is an effective candidate for light trapping in superstrate thin film nc-Si:H solar cells.

ASSOCIATED CONTENT

Supporting Information

The Supporting Information is available free of charge on the ACS Publications website at DOI: 10.1021/acsphotonics.6b00070.

Details on cell fabrication, internal quantum efficiency, and optical modeling (PDF).

AUTHOR INFORMATION

Corresponding Author

*E-mail: l.vandijk@uu.nl.

Notes

The authors declare no competing financial interest.

ACKNOWLEDGMENTS

The authors acknowledge the insightful discussions with and help of J. K. Rath, P. Spinelli, M. W. Knight, K. H. M. van der Werf, N. J. Bakker, and D. L. Perrier. We gratefully acknowledge M. Verschuuren for soft imprint advice and stamp fabrication. This work is supported by NanoNextNL, a micro- and nanotechnology consortium of the Government of The Netherlands and 130 partners. The work at AMOLF is part of the research program of the "Stichting voor Fundamenteel Onderzoek der Materie (FOM)", which is part of the "Nederlandse Organisatie voor Wetenschappelijk Onderzoek (NWO)" and is supported by the European Research Council (ERC). SURFsara is acknowledged for offering the high performance computing facilities.

REFERENCES

(1) HyET Solar. http://www.hyetsolar.nl/.

(2) Okur, S.; Güneş, M.; Finger, F.; Carius, R. Diffusion length measurements of microcrystalline silicon thin films prepared by hot-wire/catalytic chemical vapor deposition (HWCVD). *Thin Solid Films* **2006**, *501*, 137−140.

(3) Boccard, M.; Battaglia, C.; Hänni, S.; Söderström, K.; Escarré, J.; Nicolay, S.; Meillaud, F.; Despeisse, M.; Ballif, C. Multiscale transparent electrode architecture for efficient light management and carrier collection in solar cells. *Nano Lett.* **2012**, *12*, 1344−1348.

(4) Sai, H.; Saito, K.; Hozuki, N.; Kondo, M. Relationship between the cell thickness and the optimum period of textured back reflectors in thin-film microcrystalline silicon solar cells. *Appl. Phys. Lett.* **2013**, *102*, 053509.

(5) Sai, H.; Kanamori, Y.; Kondo, M. Flattened light-scattering substrate in thin film silicon solar cells for improved infrared response. *Appl. Phys. Lett.* **2011**, *98*, 113502.

(6) Sai, H.; Maejima, K.; Matsui, T.; Koida, T.; Kondo, M.; Nakao, S.; Takeuchi, Y.; Katayama, H.; Yoshida, I. High-efficiency microcrystalline silicon solar cells on honeycomb textured substrates grown with high-rate VHF plasma-enhanced chemical vapor deposition. *Jpn. J. Appl. Phys.* **2015**, *54*, 08KB05.

DOI: 10.1021/acsphotonics.6b00070
ACS Photonics 2016, 3, 685−691

(7) Polman, A.; Knight, M.; Garnett, E. C.; Ehrler, B.; Sinke, W. C. Photovoltaic materials-present efficiencies and future challenges. *Science* **2016**, Accepted for publication.
(8) Berginski, M.; Hüpkes, J.; Schulte, M.; Schöpe, G.; Stiebig, H.; Rech, B.; Wuttig, M. The effect of front ZnO: Al surface texture and optical transparency on efficient light trapping in silicon thin-film solar cells. *J. Appl. Phys.* **2007**, *101*, 074903.
(9) Bhattacharya, J.; Chakravarty, N.; Pattnaik, S.; Slafer, W. D.; Biswas, R.; Dalal, V. L. A photonic-plasmonic structure for enhancing light absorption in thin film solar cells. *Appl. Phys. Lett.* **2011**, *99*, 131114.
(10) Tan, H.; Psomadaki, E.; Isabella, O.; Fischer, M.; Babal, P.; Vasudevan, R.; Zeman, M.; Smets, A. H. Micro-textures for efficient light trapping and improved electrical performance in thin-film nanocrystalline silicon solar cells. *Appl. Phys. Lett.* **2013**, *103*, 173905.
(11) Kuang, Y.; van Lare, M.; Veldhuizen, L.; Polman, A.; Rath, J.; Schropp, R. Efficient nanorod-based amorphous silicon solar cells with advanced light trapping. *J. Appl. Phys.* **2015**, *118*, 185307.
(12) Di Vece, M.; Kuang, Y.; van Duren, S. N.; Charry, J. M.; van Dijk, L.; Schropp, R. E. Plasmonic nano-antenna a-Si:H solar cell. *Opt. Express* **2012**, *20*, 27327−27336.
(13) Vanecek, M.; Babchenko, O.; Purkrt, A.; Holovsky, J.; Neykova, N.; Poruba, A.; Remes, Z.; Meier, J.; Kroll, U. Nanostructured three-dimensional thin film silicon solar cells with very high efficiency potential. *Appl. Phys. Lett.* **2011**, *98*, 163503.
(14) Matsui, T.; Tsukiji, M.; Saika, H.; Toyama, T.; Okamoto, H. Influence of substrate texture on microstructure and photovoltaic performances of thin film polycrystalline silicon solar cells. *J. Non-Cryst. Solids* **2002**, *299*, 1152−1156.
(15) Li, H. B.; Franken, R. H.; Rath, J. K.; Schropp, R. E. Structural defects caused by a rough substrate and their influence on the performance of hydrogenated nano-crystalline silicon n-i-p solar cells. *Sol. Energy Mater. Sol. Cells* **2009**, *93*, 338−349.
(16) Schropp, R.; Rath, J.; Li, H. Growth mechanism of nanocrystalline silicon at the phase transition and its application in thin film solar cells. *J. Cryst. Growth* **2009**, *311*, 760−764.
(17) Python, M.; Dominé, D.; Söderström, T.; Meillaud, F.; Ballif, C. Microcrystalline silicon solar cells: effect of substrate temperature on cracks and their role in post-oxidation. *Prog. Photovoltaics* **2010**, *18*, 491−499.
(18) Sever, M.; Krč, J.; Topič, M. Prediction of defective regions in optimization of surface textures in thin-film silicon solar cells using combined model of layer growth. *Thin Solid Films* **2014**, *573*, 176−184.
(19) Gordijn, A.; Hodakova, L.; Rath, J.; Schropp, R. Influence on cell performance of bulk defect density in microcrystalline silicon grown by VHF PECVD. *J. Non-Cryst. Solids* **2006**, *352*, 1868−1871.
(20) Bugnon, G.; Parascandolo, G.; Söderström, T.; Cuony, P.; Despeisse, M.; Hänni, S.; Holovskỳ, J.; Meillaud, F.; Ballif, C. A new view of microcrystalline silicon: the role of plasma processing in achieving a dense and stable absorber material for photovoltaic applications. *Adv. Funct. Mater.* **2012**, *22*, 3665−3671.
(21) Söderström, K.; Bugnon, G.; Haug, F.-J.; Nicolay, S.; Ballif, C. Experimental study of flat light-scattering substrates in thin-film silicon solar cells. *Sol. Energy Mater. Sol. Cells* **2012**, *101*, 193−199.
(22) Feltrin, A.; Suezaki, T.; Meguro, T.; Ichikawa, M. Advanced super light trapping of high efficiency thin film silicon solar cells. 4th International Workshop on Thin-Film Silicon Solar Cell, Neuchatel, Switzerland, March 19−23, 2012.
(23) Schwind, M.; Kasemo, B.; Zorić, I. Localized and propagating plasmons in metal films with nanoholes. *Nano Lett.* **2013**, *13*, 1743−1750.
(24) Lacharmoise, P.; Tognalli, N.; Goñi, A.; Alonso, M.; Fainstein, A.; Cole, R.; Baumberg, J.; de Abajo, J. G.; Bartlett, P. Imaging optical near fields at metallic nanoscale voids. *Phys. Rev. B: Condens. Matter Mater. Phys.* **2008**, *78*, 125410.
(25) Reilly, T. H., III; Tenent, R. C.; Barnes, T. M.; Rowlen, K. L.; van de Lagemaat, J. Controlling the optical properties of plasmonic disordered nanohole silver films. *ACS Nano* **2010**, *4*, 615−624.
(26) Rotenberg, N.; Spasenović, M.; Krijger, T.; Le Feber, B.; de Abajo, F. G.; Kuipers, L. Plasmon scattering from single subwavelength holes. *Phys. Rev. Lett.* **2012**, *108*, 127402.
(27) Vynck, K.; Burresi, M.; Riboli, F.; Wiersma, D. S. Photon management in two-dimensional disordered media. *Nat. Mater.* **2012**, *11*, 1017−1022.
(28) Chou, S. Y.; Ding, W. Ultrathin, high-efficiency, broad-band, omni-acceptance, organic solar cells enhanced by plasmonic cavity with subwavelength hole array. *Opt. Express* **2013**, *21*, A60−A76.
(29) Ferry, V. E.; Verschuuren, M. A.; Li, H. B.; Schropp, R. E.; Atwater, H. A.; Polman, A. Improved red-response in thin film a-Si: H solar cells with soft-imprinted plasmonic back reflectors. *Appl. Phys. Lett.* **2009**, *95*, 183503.
(30) Mann, S. A.; Grote, R. R.; Osgood, R. M.; Schuller, J. A. Dielectric particle and void resonators for thin film solar cell textures. *Opt. Express* **2011**, *19*, 25729−25740.
(31) Spinelli, P.; Verschuuren, M.; Polman, A. Broadband omnidirectional antireflection coating based on subwavelength surface Mie resonators. *Nat. Commun.* **2012**, *3*, 692.
(32) Paetzold, U.; Moulin, E.; Michaelis, D.; Böttler, W.; Wächter, C.; Hagemann, V.; Meier, M.; Carius, R.; Rau, U. Plasmonic reflection grating back contacts for microcrystalline silicon solar cells. *Appl. Phys. Lett.* **2011**, *99*, 181105.
(33) Pillai, S.; Catchpole, K.; Trupke, T.; Green, M. Surface plasmon enhanced silicon solar cells. *J. Appl. Phys.* **2007**, *101*, 093105.
(34) Esfandyarpour, M.; Garnett, E. C.; Cui, Y.; McGehee, M. D.; Brongersma, M. L. Metamaterial mirrors in optoelectronic devices. *Nat. Nanotechnol.* **2014**, *9*, 542−547.
(35) Zhao, J.; Wang, A.; Green, M. 24% efficient PERL structure silicon solar cells. Photovoltaic Specialists Conference, 1990, Conference Record of the 21st IEEE, Kissimmee, FL, May 21−25, 1990; IEEE, 1990; pp 333−335.
(36) Verschuuren, M. A. Substrate Conformal Imprint Lithography for Nanophotonics. *Ph.D. Thesis*; Utrecht University, 2010.
(37) Ji, R.; Krueger, A.; Hornung, M.; Verschuuren, M.; van de Laar, R.; van Eekelen, J. Full field nanoimprint on mask aligners using substrate conformal imprint lithography technique. *Acta Phys. Pol., A* **2009**, *116*, s187−s189.
(38) Franken, R. Transparent conducting oxide contacts and textured metal back reflectors for thin film silicon solar cells. *Ph.D. Thesis*; Utrecht University, 2006.
(39) Zappe, H. *Fundamentals of Micro-Optics*; Cambridge University Press, 2010.
(40) Haug, F.-J.; Söderström, K.; Naqavi, A.; Ballif, C. Resonances and absorption enhancement in thin film silicon solar cells with periodic interface texture. *J. Appl. Phys.* **2011**, *109*, 084516.
(41) Lin, C.; Martínez, L. J.; Povinelli, M. L. Experimental broadband absorption enhancement in silicon nanohole structures with optimized complex unit cells. *Opt. Express* **2013**, *21*, A872−A882.
(42) Wang, C.; Yu, S.; Chen, W.; Sun, C. Highly efficient light-trapping structure design inspired by natural evolution. *Sci. Rep.* **2013**, *3*, 1025.
(43) van Lare, C.; Polman, A. Optimized Scattering Power Spectral Density of Photovoltaic Light-Trapping Patterns. *ACS Photonics* **2015**, *2*, 822−831.
(44) Smeets, M.; Smirnov, V.; Bittkau, K.; Meier, M.; Carius, R.; Rau, U.; Paetzold, U. W. Angular dependence of light trapping in nanophotonic thin-film solar cells. *Opt. Express* **2015**, *23*, A1575−A1588.
(45) van Dijk, L.; Paetzold, U. W.; Blab, G. A.; Schropp, R. E.; Di Vece, M. 3D-printed external light trap for solar cells. *Prog. Photovoltaics* **2016**, *24*, 623−633.

DOI: 10.1021/acsphotonics.6b00070
ACS Photonics 2016, 3, 685−691